Δ self-consistent field method for natural anthocyanidin dyes

U. Terranova and D. R. Bowler,
Department of Physics and Astronomy,
University College London, London, WC1E 6BT, U.K.;
International Center for Materials Nanoarchitectonics (MANA),
1-1 Namiki, Tsukuba, Ibaraki 305-0044, Japan

Abstract

We present an application of the Δ self-consistent field (ΔSCF) method, which we have implemented and tested in the DFT code CONQUEST, on the study of excited states of natural anthocyanidin dyes. We show that ΔSCF allows relaxation of the atomic structure for systems in excited states by following gradients on the excited Born-Oppenheimer surface. We compare the vertical excitation energies of some anthocyanidins in gas-phase to results from time-dependent density functional theory (TDDFT) and experiments. To reproduce a typical dye-sensitised solar cell interface, we adsorb cyanidin on TiO_2 anatase (101), focussing on the shift of the lowest excitation energy due to the adsorption. We have found that important modifications occur in the excited state geometry of the adsorbed cyanidin.

1 Introduction

With the increasing demand for renewable sources of energy, dye-sensitised solar cells (DSSCs) are gaining more and more attention as a viable alternative to the traditional silicon devices [1, 2]. In a DSSC, a layer of a light-harvesting dye is bound to the surface of a nanoporous TiO_2 anatase film. After the photoexcitation, an electron is transferred to the conduction band (CB) of the oxide and can be used to do some electrical work. The dye is then regenerated by a redox couple in solution, in turn reduced by the electrons passed through the load.

One of the key parameters in the development of new dyes, alternative to the expensive ruthenium based sensitisers, is the absorption spectrum, which one would like to tune to the solar spectrum. The calculation of absorption spectra is one of the main problems of computational chemistry. Time-dependent density functional theory (TDDFT) provides localised valence excitations which are usually accurate to within 0.3 eV [3, 4]. The drawback of TDDFT is the underestimation of charge transfer excitations [5], which can be addressed by introducing in the functional a growing amount of exact exchange at long range [6–8]. Alternatively, approaches like constrained DFT [9], where an external potential is added to fulfil a desired constraint on the density, have been proposed to overcome the difficulty [10–12].

Δ self-consistent field (ΔSCF) is one of the earliest methods for the calculation of excitation energies in Hartree-Fock [13, 14]. These are calculated by promoting one electron into a virtual orbital, and solving the equations for the constrained configuration. The applicability to DFT, where the excited states can be calculated by populating different Kohn-Sham eigenstates, is then straightforward [15], at a cost not very different from the ordinary ground state theory.

ΔSCF has been shown to give satisfactory results for the potential energy surfaces (PESs) of H_2 and NaCl [15], the vertical excitations of N_2 and CO [16], and CO adsorbed on Pd(111) [15]. A surprisingly similar accuracy to TDDFT has been observed for a test set of vertical excitation energies of 16 chromophores [17], and the use of ΔSCF to investigate the isomerisation dynamics of azobenzene has yielded PESs that agree very well with those derived from TDDFT [18]. Motivated by the successes reported in the literature, we have implemented ΔSCF in the DFT code CONQUEST [19–21].

Here, we first report some tests on the lowest PESs of CO and the vertical excitation energies of catechol. Then, we move to natural anthocyanidins, already employed with promising efficiencies in DSSCs [22]. Despite ΔSCF underestimating their excitation energies, the expected order of the excitations between the various dyes is reproduced. To investigate a typical DSSC interface, we have adsorbed cyanidin on TiO_2 anatase (101), focussing on the resulting shift of the excitation, which is again correctly described by ΔSCF. Finally, we show that simply taking the ΔSCF gradient allows relaxation of the atomic structure of dyes in their excited states, even in the case of a dye adsorbed on a surface.

2 The ΔSCF method in DFT

We recall that in DFT the ground state density $n(\mathbf{r})$ of a system of N electrons can be found by solving the Kohn-Sham (KS) equations:

$$H_{\mathrm{KS}}\psi_i(\mathbf{r}) = \varepsilon_i\psi_i(\mathbf{r}), \tag{1}$$

and taking the square sum of the resulting KS orbitals:

$$n(\mathbf{r}) = \sum_{i=1}^{\infty} f_i|\psi_i(\mathbf{r})|^2, \tag{2}$$

where only the lowest N orbitals contribute (f_i equals 1 if $i \leq N$, 0 otherwise). As H_{KS} is itself a functional of the density, Eq. (1) and (2) must be solved in a self-consistent way.

Once the set of the KS orbitals has been calculated, a very intuitive way to simulate an excitation in a molecule is to promote one electron from an occupied ψ_k ($k \leq N$) to a virtual orbital ψ_l ($l > N$). The new density $n^{\mathrm{exc}}(\mathbf{r})$, calculated from Eq. (2) with $f_k = 0$ and $f_l = 1$, can be used to construct an excited Hamiltonian $H^{\mathrm{exc}}_{\mathrm{KS}}(\mathbf{r})$ and set up new KS equations:

$$H^{\mathrm{exc}}_{\mathrm{KS}}\psi_i(\mathbf{r}) = \varepsilon_i\psi_i(\mathbf{r}), \tag{3}$$

These are solved again self-consistently, with the restriction of maintaining the $\psi_k \rightarrow \psi_l$ excitation at every iteration.

Within ΔSCF, the calculation of triplet energies, E_{T}, is immediate. In a system where all the orbitals are doubly occupied, except for the two highest orbitals ψ_a and ψ_r which are singly occupied by electrons of spin α, the $S_z = 1$ triplet configuration from a Slater determinant is:

$$ {}^{3}_{1}\Psi = \frac{1}{\sqrt{2}}[\psi_a(\mathbf{r}_1)\psi_r(\mathbf{r}_2) - \psi_a(\mathbf{r}_2)\psi_r(\mathbf{r}_1)]\alpha(s_1)\alpha(s_2). \tag{4} $$

Here, we have indicated with s_1 and s_2 the spin coordinates of the unpaired electrons having spatial coordinates $\mathbf{r}_1$ and $\mathbf{r}_2$, while neglected the irrelevant closed shell orbitals. ΔSCF calculates triplet energies by a self-consistent run in this spin-constrained configuration.

Excited singlet energies of dyes, E_{S}, are not directly accessible by single determinants and are thus approximated by means of the sum method [23]. In particular, in a configuration where ψ_a and ψ_r are both singly occupied by electrons of spin α and β respectively, the corresponding spin mixed configuration from a Slater determinant is:

$$ {}^{\mathrm{MIX}}\Psi = \frac{1}{\sqrt{2}}[\psi_a(\mathbf{r}_1)\beta(s_1)\psi_r(\mathbf{r}_2)\alpha(s_2) - \psi_a(\mathbf{r}_2)\beta(s_2)\psi_r(\mathbf{r}_1)\alpha(s_1)], \tag{5} $$

whose energy E_{MIX} can be calculated by a second spin-constrained ΔSCF run. Since ${}^{\mathrm{MIX}}\Psi$ is given by an equal combination of the $S_z = 0$ triplet and singlet, respectively ${}^{3}_{0}\Psi$ and ${}^{1}_{0}\Psi$:

$$ {}^{\mathrm{MIX}}\Psi = \frac{1}{2}({}^{3}_{0}\Psi + {}^{1}_{0}\Psi), \tag{6} $$

the following expression for E_{MIX} holds when the triplets are degenerate:

$$ E_{\mathrm{MIX}} = \frac{1}{2}(E_{\mathrm{S}} + E_{\mathrm{T}}). \tag{7} $$

Eq. 7 provides the formula for E_{S} commonly employed in DFT-ΔSCF [16, 18], yielding an accuracy comparable to that of TDDFT [17].

3 Computational details

We have performed the calculations with the CONQUEST code [19–21], which uses localised orbitals called support functions to represent the Hamiltonian, and can find the ground state by exact diagonalisation or in a linear scaling fashion [24]. Here, we choose diagonalisation, and let the localised orbitals take the form of pseudoatomic orbitals (PAOs). We have used the local spin density approximation (LSDA) [25], Troullier-Martins pseudopotentials [26], and a DZP basis set (15 PAOs for Ti, 13 for C and O, and 5 for H). Relaxations of structures were performed with a DIIS method [27], and stopped when the force acting on each nucleus was less than 0.05 eV/Å.

To model TiO_2 anatase (101), we have used a (1×2) surface unit cell, with a thickness of 4 Ti-layers, and dimensions of $(10.073 \times 7.450$ Å). To avoid any spurious interaction between atoms from different cells, adjacent slabs were separeted by a vacuum gap of 20 Å. We have found in Ref. [28] that a **k**-point grid of $1 \times 2 \times 1$ gives good convergence for this unit cell, and adopted it here.

State	Transition	ΔSCF	TDDFT (PBE)[30]	exp[31]
$X^1\Sigma^+$	-	1.13	-	1.128
$A^1\Pi$	$5\sigma \rightarrow 2\pi$	1.22	1.24	1.235
$a^3\Pi$	$5\sigma \rightarrow 2\pi$	1.21	1.20	1.206
$D^1\Delta$	$1\pi \rightarrow 2\pi$	1.44	1.38	1.399
$d^3\Delta$	$1\pi \rightarrow 2\pi$	1.38	1.38	1.370
$c^3\Pi$	$4\sigma \rightarrow 2\pi$	1.28	1.25	1.348

Table 1: Equilibrium bond lengths (Å) of the ground ($X^1\Sigma^+$) and lowest excited states of CO.

By means of ΔSCF, we reproduce an excitation from the highest occupied to the lowest unoccupied level of the dye, i.e. a $\mathrm{HOMO_{dye}} \rightarrow \mathrm{LUMO_{dye}}$ excitation, typical of sensitisers in DSSCs. Since during the self-consistent procedure the position of $\mathrm{HOMO_{dye}}$ and $\mathrm{LUMO_{dye}}$ with respect to the TiO_2 levels can change, it is important to determine at every iteration $\mathrm{HOMO_{dye}}$ and $\mathrm{LUMO_{dye}}$ and update the occupancies of these levels.

To this end, we search the KS orbitals in a user-specified range below HOMO and above LUMO, and expand them with respect to the PAOs:

$$\psi_j = \Sigma_\alpha c_{j\alpha}\phi_\alpha + \Sigma_\beta c_{j\beta}\phi_\beta, \tag{8}$$

where ϕ_α and ϕ_β are the PAOs centred on the atoms of the dye or the oxide, respectively. By summing over the squared coefficients $|c_{j\alpha}|^2$ and $|c_{j\beta}|^2$ we obtain two coefficients which reflect the localisation of a given KS orbital, ψ_j, on the dye:

$$D_j = \Sigma_\alpha |c_{j\alpha}|^2, \tag{9}$$

and on the surface:

$$O_j = \Sigma_\beta |c_{j\beta}|^2. \tag{10}$$

By comparing these, we can assign the orbitals, during the self consistent cycle, either to the dye or the surface, and dynamically localise $\mathrm{HOMO_{dye}}$ and $\mathrm{LUMO_{dye}}$.

4 Testing ΔSCF

4.1 CO molecule

CO is a simple molecule to test the implementation of ΔSCF, with existing results from previous ΔSCF calculations [16]. For this dimer, we have studied the ground and a few excited singlet and triplet PESs, from which we have extracted the vertical excitation energies and the position of the minima.

We have taken the transition configurations of the excited states from a previous TDDFT work [29] with the LDA functional. As both the 1π and 2π orbitals are doubly degenerate, when involved in the excitations, we have removed or added half electron in each of them. We have found a DZP basis set not enough to achieve convergence, and the results presented have been obtained with a triple-ζ double polarised basis set (22 PAOs for both C and O).

From the PESs of Figure 1, we have obtained the equilibrium bond lengths (Table 1), and the vertical excitation energies (Table 2), in qualitative agreement

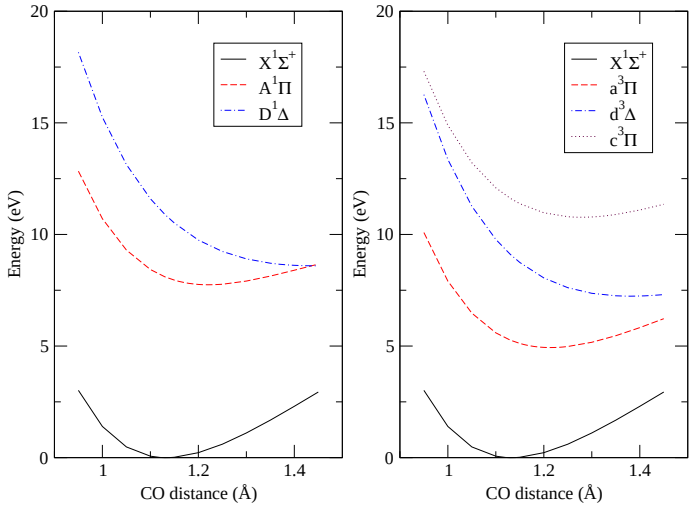

Figure 1: Potential energy surfaces for the ground and the lowest singlet (left) and triplet (right) excited states of CO obtained by ΔSCF.

State	Transition	ΔSCF	ΔSCF (LDA)[16]	TDDFT (LDA)[29]	exp[31]
$A^1\Pi$	$5\sigma \rightarrow 2\pi$	8.10	7.84	8.25	8.51
$a^3\Pi$	$5\sigma \rightarrow 2\pi$	5.26	6.09	6.02	6.32
$D^1\Delta$	$1\pi \rightarrow 2\pi$	10.90	10.82	10.02	10.23
$d^3\Delta$	$1\pi \rightarrow 2\pi$	9.11	9.72	9.24	9.36
$c^3\Pi$	$4\sigma \rightarrow 2\pi$	11.62	12.26	11.43	11.55

Table 2: Vertical excitation energies (eV) of the lowest excited states of CO.

with TDDFT [29, 30] and experiment [31]. Our ΔSCF implementation differs to that of the previous work [16] in the use of PAOs instead of plane waves, and some discrepancy is thus expected. The agreement with the literature is however very good, and we are confident in the implementation of the method.

4.2 Free and Ti-bound catechol

As a second test, we have calculated the excitation energies of free and Ti-bound catechol (Figure 2), a dye which can be used as an efficient ligand for the attachment of larger sensitisers [32].

The lowest energy band $S_0 \rightarrow S_1$ of free catechol is dominated by a HOMO → LUMO transition [33, 34]. Experimentally, the catechol-Ti binding in an aqueous solution does not cause any shift of the spectrum, but a new low energy $S_0 \rightarrow$ Ti band appears. [35]. In the Ti-bound catechol, the excitation corresponding to $S_0 \rightarrow S_1$ is between orbitals which are nearly identical to those of

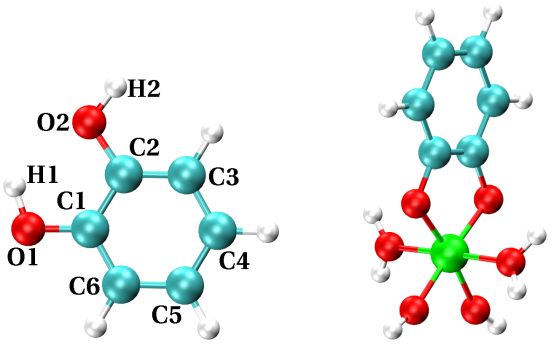

Figure 2: Structure of free (left) and Ti-bound (right) catechol. The latter corresponds to the expected neutral species in aqueous solution [33].

	Free	Ti-bound
KS	4.10	4.17
ΔSCF	4.50	4.41
TDDFT (PW91)[33]	4.77	4.86
TDDFT (B3LYP)[33]	5.06	5.08
Exp[35]	4.59	4.59

Table 3: Lowest intramolecular excitation energies (eV) of free and Ti-bound catechol compared to the results in the literature.

free catechol [33]. The vertical excitations of free and Ti-bound catechol are presented in Table 3, together with previous results from the literature. In both systems, ΔSCF improves the KS difference between $\mathrm{HOMO_{dye}}$ and $\mathrm{LUMO_{dye}}$, and reproduces the position of the peak with good accuracy.

As well as the calculation of excitation energies, an interesting application of ΔSCF is the relaxation of a molecule in its excited state. To this end, we can make use of the Hellmann-Feynman theorem to find forces, and relax the structure in the excited Born-Oppenheimer surface without any significant modification of the main DFT code.

After updating the nuclei, one could solve again for the ground state density and then re-excite the electron, or look directly for self-consistency of the excited state density. We have chosen the second approach, as tests have shown that it halves the computational time, while the differences in all of the bond lengths between the two procedures are always less than 0.01 Å.

We have mentioned that the lowest optical band of free catechol is dominated by a single electronic excitation, primarily of the HOMO → LUMO origin [33, 34]. Accordingly, we have employed HOMO and LUMO of the same spin channel to promote the electron and relax the dye by ΔSCF.

The deviations of the main geometrical parameters of catechol from the ground state are reported in Table 4, where they are compared with some previous results from the literature [36]. We find the benzene ring to be planar. The most important changes are given by the increase of all of the CC bond distances. On the other hand, the CO lengths become smaller. Also the bond angles modify their values, with differences up to almost 6 degrees for C2C3C4 and

Bonds	TDDFT (PW91PW91)[36]	ΔSCF
C1C2	+0.02	+0.01
C2C3	+0.04	+0.04
C3C4	+0.00	+0.02
C4C5	+0.02	+0.02
C5C6	+0.00	+0.01
C6C1	+0.04	+0.05
C1O1	−0.02	−0.02
C2O2	−0.01	−0.02
Angles		
C1C2C3	+0.6	+2.2
C2C3C4	−3.0	−5.8
C3C4C5	+1.9	+3.6
C4C5C6	+1.6	+2.6
C5C6C1	−3.1	−5.7
C6C1C2	+1.4	+3.1
O1C1C2	+0.3	−0.3
O2C2C3	−2.7	−2.4
Dihedrals		
H1O1C1C2	+11.6	+1.2
H2O2C2C3	+5.9	+25.0

Table 4: Deviation from the ground state of the most important parameters of catechol in the first excited state compared to the results in the literature. Values for bonds are expressed in Å, for angles and dihedrals in degrees. Labels refer to Figure 2.

C5C6C1. With the exception of the two dihedrals H1O1C1C2 and H2O2C2C3, the described trend agrees very well with the one in the literature [36], and suggests that ΔSCF can be used as a simple tool for the calculation of excited state geometries.

At this point, we would like to report an unsuccessful attempt to test ΔSCF for catechol adsorbed on TiO_2 anatase (101), a model interface for DSSCs. In our calculations, $LUMO_{dye}$ corresponds to LUMO+43, and has an energy of 4.82 eV with respect to the bottom of the CB of the oxide. $LUMO_{dye}$ mixes with the continuum of levels of TiO_2, as indicated by its expansion coefficients D_L and O_L (Eqs. 9 and 10), respectively 1.0 and 0.5 for catechol and TiO_2. In this case, an assignment of $LUMO_{dye}$ based on the physical localisation of the orbitals is necessarily weak. Moreover, during the self-consistent run in S_1, the position of $LUMO_{dye}$ varies discontinuously, because the values of D_j and O_j are very close to each other, and oscillate in many orbitals. We believe that the hybridisation of the $LUMO_{dye}$ with the continuum of states of the oxide is the source of lack of self-consistency.

One possible way to tackle the problem could be to extend ΔSCF to allow excited electrons to occupy linear combinations of KS states. This approach has been shown to perform better than standard ΔSCF when the molecular orbitals hybridise with the surface [16]. Different strategies to improve convergence are

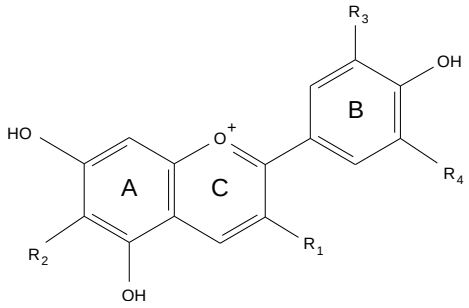

Figure 3: Chemical structure of the anthocyanidins studied in this work.

Name	R_1	R_2	R_3	R_4
Pelargonidin	OH	H	H	H
Cyanidin	OH	H	OH	H
Delphinidin	OH	H	OH	OH
Aurantinidin	OH	OH	H	H

Table 5: Anthocyanidins used in this work according to their substitutions.

the use of fractionally occupied orbitals in the self-consistent run [37], or the implementation of alternative schemes within DIIS, such as EDIIS [38], ADIIS [39], LISTi [40], LISTb [41], to accelerate the convergence. In particular, among the possible methods, a combination of both DIIS and EDIIS is usually the most efficient [42].

However, we are not directly concerned with catechol in this work, and have not pursued any of these routes. As shown in section 5.3, we have not experienced any issues in the adsorption of the cyanidin dye. For the latter, $\mathrm{LUMO}_{\mathrm{dye}}$ is always situated below the CB, and two orders of magnitude separate D_L from O_L.

5 Anthocyanidins

Now we turn to an application of the method to systems which are relevant to DSSCs. Anthocyanins and anthocyanidins are phenolic compounds responsible for the colour of many fruits and vegetables. Since very common in nature, they have been both traditionally employed in DSSCs, with low but promising efficiencies up to 1% [22, 43–46]. Anthocyanidins consist of two aromatic rings (A and C) bonded to a third aromatic ring (B) (Fig. 3). If a sugar group is present at position R_1, anthocyanidins are known as anthocyanins, whose optical properties are very similar [47]. Here, to reduce the computational cost, all of the calculations have been carried out with the sugar free compounds.

5.1 Effect of hydroxylations

In agreement with experiments [48, 49], *ab initio* configuration interaction (CI) calculations have shown that hydroxy substitutions at position R_2 increase the lowest excitation energy in anthocyanidins, while successive hydroxylations at

Name	KS	ΔSCF	TDDFT (B3P86)[51]	CI[50]	Exp[48]
Pelargonidin	1.70	1.74	2.55	2.58	2.38
Cyanidin	1.61	1.67	2.46	2.56	2.32
Delphinidin	1.64	1.57	2.50	2.46	2.27
Aurantinidin	1.72	1.86	-	2.63	2.48

Table 6: Lowest excitation energies (eV) of anthocyanidins compared to the results in the literature.

positions R_3 and R_4 decrease it [50].

To assess the performance of ΔSCF, we have studied the lowest excitation energies of the anthocyanidins in Ref. [50] (Table 5). The excitations have been modelled by promoting one electron from HOMO to LUMO, as TDDFT calculations have shown that the lowest energy transition in anthocyanidins is essentially HOMO → LUMO [51].

Since we have modelled the anthocyanidins in their protonated form, a uniform background charge is introduced, and the convergence of the energy with respect to the size of the supercell is slow, reflecting the decreasing interaction between the dyes and the jellium background. However, excitation energies are given by differences of energies, and in our calculations, they are already converged to within 0.01 eV with respect to the size of the supercell.

Results are presented in Table 6, where they are compared with other works in the literature. ΔSCF severely underestimates the experimental values by around 0.5 eV, which could be ascribed to the LDA problem with optical gaps (in TDDFT, hybrid functionals shift the peaks of anthocyanidins by 0.3–0.4 eV with respect to the PBE functional [47, 52]). A direct comparison with the experimental data is however not possible, as they were taken with dyes in a methanol solvent. We note that while TDDFT gives energies which are close to the experiments, it fails in reproducing the correct relative order. On the contrary, despite the severe underestimation, ΔSCF follows the expected trend, i.e., a hydroxylation in the A-ring causes a blue-shift in the spectrum, while a red-shift is the consequence of successive hydroxy substitutions in the B-ring.

5.2 Effect of pH

The chemical form of anthocyanins is dependent on the pH of the solution (Figure 4). At acidic conditions (pH < 3), anthocyanins exist mostly in the protonated flavylium form (AH^+), and present an absorption band at 2.34 eV [53]. In the pH range 3–4, the flavylium coexists with a neutral quinonoidal form (A), whose absorption band is red-shifted to 2.24 eV. Then, up to pH 5 the quinonoidal form is prevalent. At higher pH, an ionised quinonoidal form (A^-) also appears.

We have calculated the ΔSCF excitation energies of cyanidin for AH^+, A, and A^- (Table 7). Our calculations indicate that, from the neutral form A, a protonation shifts the excitation energies towards the red, in agreement with TDDFT, but at odds with the experiment. An increase of pH red-shifts the spectrum too, in agreement with both TDDFT and experiment.

So far, the emerging picture is that LDA-ΔSCF underestimates the excitation energies of anthocyanidins. A study on the singlet states of a set of 16

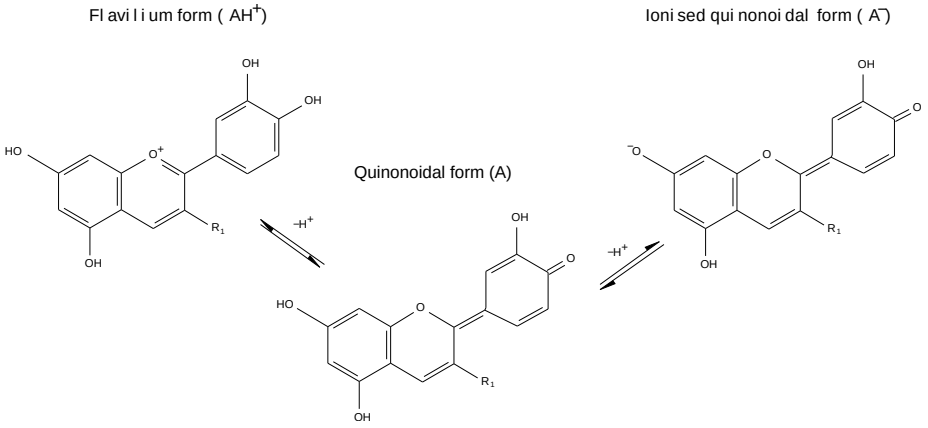

Figure 4: Equilibrium between the various forms of cyanin depending on the pH of the solution.

	AH^+	A	A^-
KS	1.61	1.49	1.30
ΔSCF	1.67	1.75	1.30
TDDFT (PBE)[47]	2.14	2.33	2.20
Exp[53]	2.34	2.14	2.10

Table 7: Excitation energies (eV) of flavylium (AH^+), quinonoidal (A), and ionised quinonoidal (A^-) form of cyanidin. Experimental data refer to the anthocyanin pigment of red cabbage.

Mode	E_{ads}
MON1	−1.99
MON2	−2.87
BRI	−2.36

Table 8: Adsorption energies (eV) of the investigated modes of cyanidin on anatase (101). See text for the abbreviations of modes.

	Free	aMON1	aMON2	aBRI
KS	1.61	1.41 (0.20)	1.10 (0.51)	1.11 (0.50)
ΔSCF	1.67	1.56 (0.11)	1.42 (0.25)	1.34 (0.33)
TDDFT (PBE)[54]	2.39	-		1.91 (0.48)
Exp[22]	2.30	-		2.10 (0.20)

Table 9: Lowest excitation energies (eV) of cyanidin in gas phase and when bound to TiO_2 anatase (101). In parenthesis, the shift between the two values is reported.

chromophores [17] has revealed that when hybrid functionals are used, TDDFT and ΔSCF give similar accuracies, whereas with PBE, instead, TDDFT is on average more accurate by around 0.2 eV. As stressed by the authors, however, this is a statistical argument, and one should not expect the same accuracy between TDDFT and ΔSCF for a single class of dyes. For this reason, even with hybrid functionals, the two methods can differ also by as much as 0.6 eV [17].

5.3 Cyanidin on TiO_2 anatase (101)

Following the adsorption on TiO_2, the equilibrium between the forms is thought to be shifted towards the quinonoidal, since the cyanidin-sensitised TiO_2 appears purple and the spectrum is red-shifted by 0.20 eV compared to cyanidin in solution [22].

To investigate the effect of binding to TiO_2 on the excitation energy, we have adsorbed cyanidin on anatase (101), the most exposed face of nanoparticles in DSSCs.

5.3.1 Ground state structures

We have studied two partially dissociative monodentate (MON1 and MON2) and a fully dissociative bridging mode (BRI) (Figure 5). MON1 and BRI have a similar spatial arrangement of the dyes, while MON2 differs in their orientation. In MON1 and MON2, rather than positioning the dissociated proton on the surface, we have preferred to remove it and work with a neutral supercell. For consistency, the second dissociated proton of BRI was attached to the surface.

Table 8 reports the corresponding adsorption energies. MON2 is predicted to be the most stable binding, followed by BRI. However, when comparing the two structures with the similar spatial arrangement of the dyes, MON1 and BRI, the latter is more favoured by 0.37 eV.

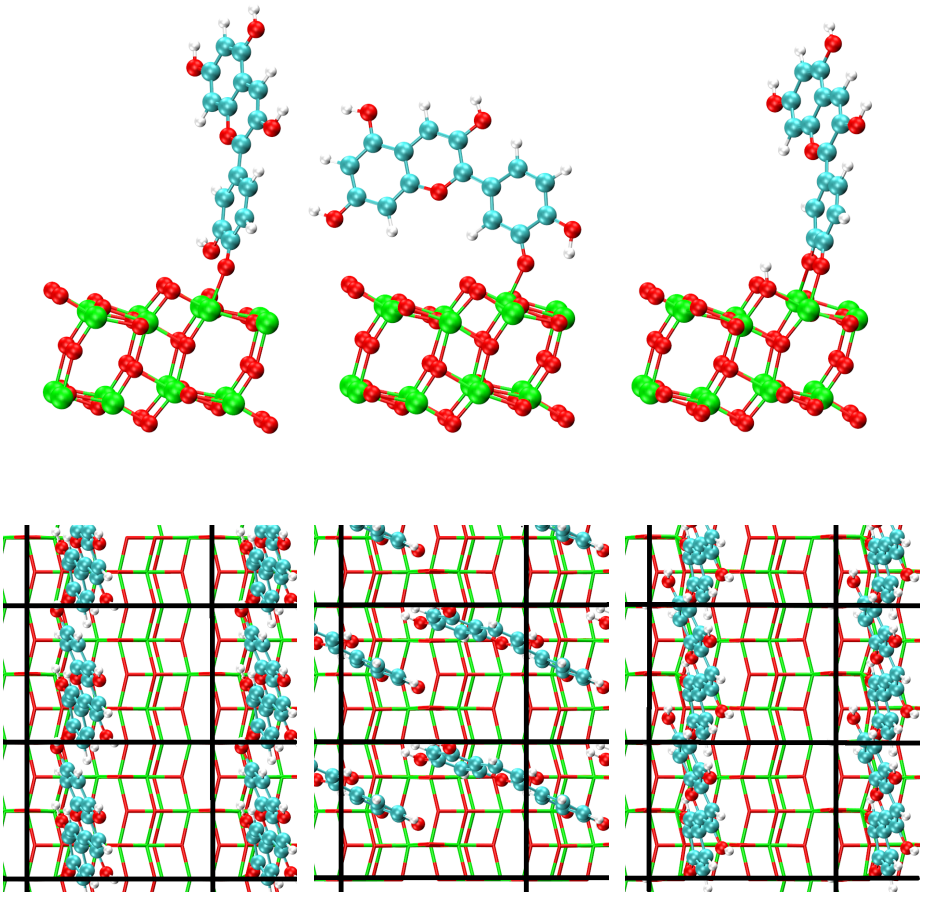

Figure 5: Front views (top) of the relaxed geometries of cyanidin on TiO_2 anatase (101) in MON1 (left), MON2 (middle), and BRI (right), with their corresponding views from the top (below). The black lines mark the periodic unit cells.

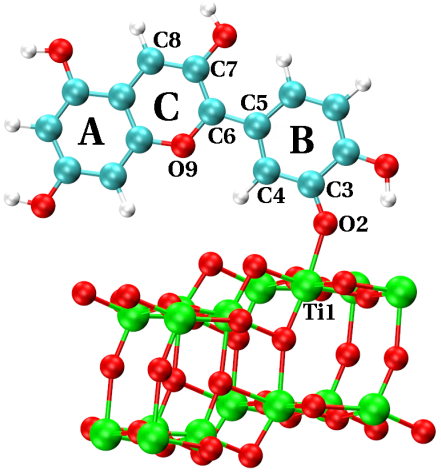

Figure 6: Excited state structure of MON2 with the atomic labels used in the text. The corresponding ground state structure is shown in Figure 5, middle.

5.3.2 Excitation energies

In Table 9, we compare the $\mathrm{HOMO_{dye}} \rightarrow \mathrm{LUMO_{dye}}$ excitation energies of cyanidin on anatase with the HOMO $\rightarrow$ LUMO of the dye in gas phase, and report the shifts caused by the binding. We show also the data from a simple KS analysis and TDDFT [54]. ΔSCF improves the KS results in all of the adsorptions, but the excitations remain far from the experimental values, which are better reproduced by TDDFT. Despite the accuracy on the excitation energies, however, TDDFT overestimates the experimental shift (0.48 vs 0.20 eV), whereas ΔSCF gives more accurate values for all of the adsorptions (0.1–0.3 eV).

5.3.3 Excited state structure of MON2

Finally, we have relaxed the most stable MON2 structure in the excited spin-mixed state by promoting one electron from $\mathrm{HOMO_{dye}}$ to $\mathrm{LUMO_{dye}}$ within the same spin channel and taking the ΔSCF gradient.

We show in Figure 6 the relaxed structure. None of the atoms of the surface displaces by more than 0.01 Å, in line with the fact that the excitation is localised within the dye. The only exception is the Ti1 atom. Its covalent bond length with the dye is increased significantly by 0.06 Å, which suggests that the interaction becomes weaker after the excitation. Another change is due to the larger distance C5C6 between the rings B and C, which increases by 0.02 Å. We have not observed any change larger than 0.01 Å also in the atoms of ring A. The most important deviations in the bond distances of cyanidin from its ground state are summarised in Table 10.

Bond	Deviation
Ti1O2	+0.06
C3C4	+0.02
C4C5	−0.02
C5C6	+0.02
C6C7	−0.03
C7C8	+0.02
C6O9	+0.02

Table 10: Most important changes (Å) in the bond lengths of the first excited state of MON2 from the ground state structure. Labels refer to Figure 6.

6 Conclusions

We have presented an implementation and assessment of the ΔSCF method, and studied its performance when applied to natural anthocyanidin dyes. We found that, for the common dye-terminating group catechol, the method performs very well, both for free and Ti-bound molecules. For the anthocyanidins, the absolute excitation energies are systematically underestimated, though the *relative* excitations between different anthocyanidins follow the experimental trend.

We have also applied this method to geometric relaxations of excited state cyanidin bound to an anatase (101) surface. Our DFT calculations predict that the most stable adsorption mode of cyanidin on TiO_2 is monodentate. While absolute $HOMO_{dye} \rightarrow LUMO_{dye}$ excitation energies are not accurate for this system, the ΔSCF description of the red-shifts from gas phase is in line with experiments. ΔSCF also represents a simple tool to calculate excited state geometries of dyes. At the affordable computational cost of DFT, we have relaxed the excited state ($HOMO_{dye} \rightarrow LUMO_{dye}$) structure corresponding to the most favoured adsorption of cyanidin on TiO_2, showing that important geometrical changes occur after the excitation.

It is not clear whether the use of hybrid functionals would correct the underestimation of excitation energies (as found on average from a study of singlet energies of organic chromophores [17], which gave an accuracy comparable to TDDFT). We also note that, despite its simplicity, the method did not allowed us the study of the catechol/anatase (101) system, due to the non-convergence of the self-consistent run in the excited state. One way to overcome the problem could be to extend ΔSCF to allow the excited electron to be spread over a linear combinations of KS states [16]. As results on free and Ti-bound catechol suggest the suitability of ΔSCF for this dye, this is a worthwhile direction.

Finally, we would like to emphasise that *ab initio* MD simulations in the excited Born-Oppenheimer state of the dye/TiO_2 system, although not performed in this work, are also possible by ΔSCF. Similarly to geometry optimisations, ΔSCF *ab initio* MD does not require any significant modification of the main code. We believe that the method is an important potential approach to the exploration of excited state geometries.

Acknowledgements

UT and DRB acknowledge financial support from the MANA-WPI project. We are grateful to Angelos Michaelides and Conn O'Rourke for stimulating discussions.

References

[1] O'Regan, B.; Grätzel, M. *Nature* **1991**, *353*, 737–740.

[2] Grätzel, M. *Nature* **2001**, *414*, 338–344.

[3] Jacquemin, D.; Wathelet, V.; Perpete, E.; Adamo, C. *J. Chem. Theory Comput.* **2009**, *5*, 2420.

[4] Guillaumont, D.; Nakamura, S. *Dyes Pigments* **2000**, *46*, 85–92.

[5] Dreuw, A.; Head-Gordon, M. *J. Am. Chem. Soc.* **2004**, *126*, 4007–4016.

[6] Leininger, T.; Stoll, H.; Werner, H.; Savin, A. *Chem. Phys. Lett.* **1997**, *275*, 151–160.

[7] Toulouse, J.; Colonna, F.; Savin, A. *Phys. Rev. A* **2004**, *70*, 062505.

[8] Jacquemin, D.; Perpète, E.; Vydrov, O.; Scuseria, G.; Adamo, C. *J. Chem. Phys.* **2007**, *127*, 094102.

[9] Dederichs, P.; Blügel, S.; Zeller, R.; Akai, H. *Phys. Rev. Lett.* **1984**, *53*, 2512–2515.

[10] Wu, Q.; Van Voorhis, T. *J. Chem. Theory Comput.* **2006**, *2*, 765–774.

[11] Sena, A.; Miyazaki, T.; Bowler, D. *J. Chem. Theory Comput.* **2011**, *7*, 884–889.

[12] Oberhofer, H.; Blumberger, J. *J. Chem. Phys.* **2009**, *131*, 064101.

[13] Gunnarsson, O.; Lundqvist, B. *Phys. Rev. B* **1976**, *13*, 4274.

[14] Jones, R.; Gunnarsson, O. *Rev. Mod. Phys.* **1989**, *61*, 689.

[15] Hellman, A.; Razaznejad, B.; Lundqvist, B. *J. Chem. Phys.* **2004**, *120*, 4593–4602.

[16] Gavnholt, J.; Olsen, T.; Engelund, M.; Schiøtz, J. *Phys. Rev. B* **2008**, *78*, 075441.

[17] Kowalczyk, T.; Yost, S.; Voorhis, T. *J. Chem. Phys.* **2011**, *134*, 054128–054128.

[18] Maurer, R.; Reuter, K. *J. Chem. Phys.* **2011**, *135*, 224303.

[19] Bowler, D.; Miyazaki, T.; Gillan, M. *J. Phys.: Condens. Matter* **2002**, *14*, 2781.

[20] Bowler, D.; Choudhury, R.; Gillan, M.; Miyazaki, T. *Phys. Status Solidi B* **2006**, *243*, 989–1000.

[21] Miyazaki, T.; Bowler, D.; Choudhury, R.; Gillan, M. *J. Chem. Phys.* **2004**, *121*, 6186.

[22] Tennakone, K.; Kumarasinghe, A.; Kumara, G.; Wijayantha, K.; Sirimanne, P. *J. Photochem. Photobiol. A* **1997**, *108*, 193–195.

[23] Ziegler, T.; Rauk, A.; Baerends, E. *Theor. Chim. Acta* **1977**, *43*, 261–271.

[24] Bowler, D.; Miyazaki, T. *Rep. Prog. Phys.* **2012**, *75*, 036503.

[25] Perdew, J.; Wang, Y. *Phys. Rev. B* **1992**, *45*, 13244–13249.

[26] Troullier, N.; Martins, J. *Phys. Rev. B* **1991**, *43*, 1993–2006.

[27] Bowler, D.; Gillan, M. *Chem. Phys. Lett.* **2000**, *325*, 473–476.

[28] Terranova, U.; Bowler, D. *J. Phys. Chem. C* **2012**, *116*, 4408–4415.

[29] Grabo, T.; Petersilka, M.; Gross, E. *J. Mol. Struct. (Theochem)* **2000**, *501*, 353–367.

[30] Marshall, D. *J. Quant. Spectrosc. Radiat. Transfer* **2008**, *109*, 2546–2560.

[31] Nielsen, E.; Jørgensen, P.; Oddershede, J. *J. Chem. Phys.* **1980**, *73*, 6238.

[32] Rice, C.; Ward, M.; Nazeeruddin, M.; Grätzel, M. *New J. Chem.* **2000**, *24*, 651–652.

[33] Duncan, W.; Prezhdo, O. *J. Phys. Chem. B* **2005**, *109*, 365–73.

[34] Sánchez-de Armas, R.; San-Miguel, M.; Oviedo, J.; Márquez, A.; Sanz, J. *Phys. Chem. Chem. Phys.* **2011**, *13*, 1506–1514.

[35] Wang, Y.; Hang, K.; Anderson, N.; Lian, T. *J. Phys. Chem. B* **2003**, *107*, 9434–9440.

[36] Cornard, J.; Lapouge, C.; Allet-Bodelot, C. *Chem. Phys. Lett.* **2010**, *489*, 164–168.

[37] Rabuck, A.; Scuseria, G. *J. Chem. Phys.* **1999**, *110*, 695.

[38] Kudin, K.; Scuseria, G.; Cancès, E. *J. Chem. Phys.* **2002**, *116*, 8255.

[39] Hu, X.; Yang, W. *J. Chem. Phys.* **2010**, *132*, 054109.

[40] Wang, Y.; Yam, C.; Chen, Y.; Chen, G. *J. Chem. Phys.* **2011**, *134*, 241103.

[41] Chen, Y.; Wang, Y. *J. Chem. Theory Comput.* **2011**, *7*, 3045–3048.

[42] Garza, A.; Scuseria, G. *J. Chem. Phys.* **2012**, *137*, 054110.

[43] Hao, S.; Wu, J.; Huang, Y.; Lin, J. *Sol. Energy* **2006**, *80*, 209–214.

[44] Calogero, G.; Marco, G. *Sol. Energy Mater. Sol. Cells* **2008**, *92*, 1341–1346.

[45] Dai, Q.; Rabani, J. *J. Photochem. Photobiol. A* **2002**, *148*, 17–24.

[46] Cherepy, N.; Smestad, G.; Grätzel, M.; Zhang, J. *J. Phys. Chem. B* **1997**, *101*, 9342–9351.

[47] Calzolari, A.; Varsano, D.; Ruini, A.; Catellani, A.; Tel-Vered, R.; Yildiz, H.; Ovits, O.; Willner, I. *J. Phys. Chem. A* **2009**, *113*, 8801–8810.

[48] Harborne, J. *Biochem. J.* **1958**, *70*, 22.

[49] Jurd, L.; Harborne, J. *Phytochemistry* **1968**, *7*, 1209–1211.

[50] Sakata, K.; Saito, N.; Honda, T. *Tetrahedron* **2006**, *62*, 3721–3731.

[51] Anouar, E.; Gierschner, J.; Duroux, J.; Trouillas, P. *Food Chem.* **2012**, *131*, 79–89.

[52] Malcıoglu, O.; Calzolari, A.; Gebauer, R.; Varsano, D.; Baroni, S. *J. Am. Chem. Soc.* **2011**.

[53] Wolf, F. *Physiol. Plant.* **1956**, *9*, 559–566.

[54] Meng, S.; Ren, J.; Kaxiras, E. *Nano Lett.* **2008**, *8*, 3266–3272.